Riaza.doc, Windows 98, Word 97

SPECTRAL MAPPING OF ROCK WEATHERING DEGREES ON GRANITE USING HYPERSPECTRAL DAIS 7915 SPECTROMETER DATA

RIAZA[a], P. STROBL[b], U. BEISL[b], A. HAUSOLD[b], A. MÜLLER[b]

[a] Geological Survey of Spain (ITGE)

Rios Rosas 23, 28003 Madrid, Spain.

Tf: 3491-3495907, Fax: 3491-4426216, E-mail:ariaza@lander.es

[b] DLR_ German Aerospace Research Establishment, German Remote Sensing Data Centre, Oberpfaffenhofen

Postfach 1116, 82230 Weßling, Germany

Keywords: day and night thermal infrared, erosion, geology, mapping, mineralogy, soil.

Abstract

Rocks are weathered by chemical and physical processes to a mixture of loose material to produce soil. Mineralogical and textural changes are involved, which can be detected by the imagery through digital image processing based on their spectral behaviour recorded by ground and laboratory spectrometers. Different densities and units of vegetation cover can be mapped qualifying further evolution of the area in terms of erosion, transport and sedimentation. Hyperspectral imagery helps to map the weathering front and different degrees of weathering granite rock through mineralogical and textural associations related to the geomorphological processes in the area. Such maps contribute to estimate the spatial controls of erosion suggesting soil particle size distribution, soil aggregation, soil depth, and consequently, helping to elaborate soil loss and soil conservation maps.

1. Introduction

Weathering processes, wether chemical or physical, produce rock disintegration. Chemical weathering releases into solution salts that remain within the weathering profiles and drainage basins for extended periods. Some are eventually precipitated preventing water infiltration. As a destructive process, weathering is an essential precursor to erosion. The weathering front separates the still fresh rock from the weathered mantle, saprolith or regolith, including the veneer of transported alluvial and colluvial debris. In granitic rocks, usually of low permeability, there is a sharp break, and most granite forms are essentially exposed weathering forms (Twidale, 1982).

Mineral reactions take place at grain contacts in dry conditions, but penetration by moisture produces more widespread effects. Water reacts with feldspar to produce clays, and acid weathering and soil conditions conducive to silica solution are implied in granitic weathering. The degree of deformation and crystal stress of the rock influences also the degree of weathering. Stressed rocks are more easily dissolved than relaxed ones. The typical end-product of the chemical weathering of granitic rocks is a gritty, puggy clay. The grittiness is due to the contained fragments and crystals of quartz. The clays, the products of the alteration of feldspars and micas, are coloured or brown or grey, according to the degree of oxidation of iron.The transportation of the weathered rock is largely the work of wash, rills and rivers. Fractures controll subsurface weathering followed by differential erosion of the unevenly weathered mass. Soil water infiltration depends on its mineralogy, texture and geomorphological setting.

Satellite imagery has been widely used to map geological features at different scales. The use of the diagnostic absorptions of electromagnetic energy in the visible and near-infrared for mineral identification has a long tradition since the study of moon dust during the Apolo campaign. Rock powdered samples have been studied, emphasizing on ultrabasic rocks, more similar to the moon dust. Various spectral libraries of minerals and rocks have been built,

which are now of public domain and well known by the geological community (Clark et al, 1993; Grove et al, 1992; Salisbury et al, 1992).

The surface of the earth is mainly covered by rocks, soil and vegetation. On non vegetated areas, rocks and soil offer the more extensive surface to airborne platforms. Both are aggregates of different mineral substances whose spectral properties are highly dependant, not only of the quantitative and qualitative mineral composition of the mixture, but of its texture and aspect at every scale. Rocks exposed to the atmosphere exhibit a weathered surface whose spectral properties differ from fresh surfaces (Riaza, 1992). Iron and clay climate-dependent weathering alteration products have been mapped based on their spectral mineralogical features (Riaza et al, 1995, 2000). Different stages on weathering products and textures have been used for relative dating of lava flows of the same chemical and mineralogical composition with thermal infrared data (Kahle et al, 1988; Abrams et al, 1991). The spectral behaviour of rocks and the effects of weathering has been studied in the thermal infrared (Ninomiya et al, 1997). Rocks, particularly intrusive rocks as granite, are covered inhomogeneously by lichen. The spectral influence of lichen cover on varyingly weathered rock surfaces has also been considered (Rollin et al, 1990), as well as different soil crusts in arid lands (O´Neill, 1994).

The study of land degradation and soil using remote sensing has a long tradition (Hill, 1993). Soil reflectance is a cumulative property deriving from the heterogeneous combination of mineral, organic and fluid matter that comprises mineral soil (Stoner & Baumgardner, 1981) and numerous studies exist about the relative contributions of parameters to reflectance of naturally occurring soils. Thermal infrared studies on soil are concentrated on the effects of particle size (Salisbury and D´Aria, 1992) and grain-size distribution and “disturbance” by packing and coatings due to wind and water transport (Johnson et al, 1998), as features playing a significant role in erosion potential.

The airborne hyperspectral Spectrometer DAIS 7915 is provided with 72 channels in the visible and near-infrared (4-2,5 μm) and 7 in the thermal infrared (8-12,5 μm) (Müller &

Oertel, 1997). Such spectral record can be compared with both field and laboratory spectrometers, introducing new possibilities for image processing and mapping capabilities. Day and night data help to evaluate the difference on the spectral behaviour of thermal infrared data.

2. Geomorphological Setting

The area of study is covered by a mass of granite where different rock facies outcrop. It is a nonpopulated grazing domain in the neighbourhood of small human settlements, subject to a mediterranean climate with dry summer and winter and relatively short rainy seasons in fall and spring. Periods of drought are recurrent within the lapse of five years. The topographically high area is covered by heterogeneous spots of evergreen oak trees and bushes, leaving wide spaces where grass grows in the short yearly rainy periods.

In every granite facies, soil close to the outcrop are darker in colour and lower in reflectance. Also, they tend to show an upper fine layer of quartz grains of different sizes dependent on the granite facies. Away from the outcrop, the grain size of the surface diminishes, and the percentage of clays increases. The central part of the topographical depressions is a solid and thick soil when dry, resulting from compaction by cattle when wet in the rainy season. Quartz grains are completely absent on this topographically low central part, and abundance of clays and roots of grass favour the compaction when the soil dries during the summer. Pools of standing water form and coalesce, and sheet flow begin (Evans, 1980).

Different granite facies also display different soil development through a geomorphological control. In general terms, a deformed granite should weather more extensively than a granite with a homogeneous texture. However, in the area of study, the more deformed granite (deformed granite with feldspar) displays a more extended outcrop area, therefore less weathered (Fig. 1). Fracturing and structural lines of weakness favour weathering deeply on the vertical weak lines, leaving a wide area of outcrop in between. The granite with coarse grained quartz and a homogeneous texture (coarse grained homogeneous granite)

weathers more superficially, offering an extensive area of soil with different depths and with the shape of smooth geomorphological depressions.

The mineralogy is also responsible for subtle weathering nuances. Abondance of feldspar presents more intense weathering. The granite facies with large feldspar phenoclasts (granite with feldspar phenoclasts) offers a nearly completely weathered surface, leaving only minor outcrop areas.

The northern homogeneous granite with abondant feldspar and big muscovite and biotite crystals (granite with biotite and muscovite) displays the larger area of outcrop, with less depressions filled with soil. Therefore, the soil is darker than the remaining granite facies.

3. Mapping through image processing

Interaction between electromagnetic energy and matter results on a varied response according to the matter spectral properties. Airborne sensors like DAIS 7915 record such response as images in a series of data corresponding to different wavelengthes. The digital image processing of values bidimensionally distributed in a large number of channels develops a peculiar method known as hyperspectral analysis. The existence of numerous channels on the same wavelenth range permits a richer appreciation of the diagnostic spectral properties of features on the surface of the earth and better results through imaging spectroscopy.

Non-coherent noise was corrected after in-flight calibration (Strobl et al, 1996) to remove the sensor sensitivity effects on the 79 DAIS channels. Different spectral imaging processing tools were tested on atmospherically corrected data using a midlatitude summer profile (Richter, 1996).

Image processing on the 72 visible and nearinfrared channels is orientated initially through principal component analysis and minimum noise fraction analysis to enhance separability of different land cover surfaces. Previous masking of dense vegetation using channels 17 and 9 for a nearinfrared/red ratio, and channel 34 (1.56 μm) for water. Minimum

Noise Fraction analysis reveals major spectral differences between rock and soil (Fig. 1). Masks were produced isolating both rock and soil using the weathering front as border, enabling further discriminating analysis for different kinds of regolith and vegetation density.

The same approach was used with Minimum Noise Fraction and Principal Components analysis on thermal infrared day and night data. Minimum Noise Fraction analysis is better distinguishing on day data (Fig. 1). It is confirmed that vegetated and fresh rock surfaces are more outstandingly shown on night data, as outlined on original channels. Discriminating image processing on both day and night data mixing Minimum Noise Fraction and Principal Components on a colour composite are the best combinations to increase information. When Minimum Noise Fraction and Principal Components are run on masked images for soil or rock, the results are certainly more contrasted, but topographical information is lost, and little spectral variety is added. The colour composite using the first and second minimum noise fraction and the second principal component (BRG) computed on the six thermal infrared channels masked to isolate soil offers nuances not appreciated on the prior imagery (Fig. 1).

4. Spectral behaviour of rocks and soils in the visible and nearinfrared: field spectra, laboratory spectra and DAIS images.

Three different areas are distinguished on rock outcrops according to different degrees of weathering shown by the imagery. Fresher rock affected by pitting outcrop on the corestones, with rough surfaces with prominent quartz grains and degraded feldspar and mica, indicating recent erosion in a geological sense. Further weathering of biotite producing clays and oxidation of iron are organized on two different areas according to the colour of the iron oxides and the mineralogy of clays (granite rock with pitting, skeletal dark regolith, thin light regolith).

Where rock is no longer outcropping, different zones are spectrally distinguished among regolith with the transported alluvial and colluvial debris from the weathering front,

wrapped around the corestones with different mineralogy related to intensity of weathering. Anthropogenic influence is spectrally outstanding on disturbed areas along roads, zones of cattle concentration, and building areas. Human influence results on severe removal of iron oxides and increase of clays and quartz. The highly reflectant mineralogical mixture with a convex shape in the visible typical of anthropogenic soil is spectrally easily mappable on the imagery (Fig. 3).

The influence of vegetation, wether on rock, or regolith, is shown by a shoulder on 0.63 μm (DAIS channel 9) (Fig. 2). The influence of lichen dominates the spectral response of the rock surface on granite, both on overall reflectance and spectral absorptions (Rollin et al, 1990). After observations on field spectra with a GER Spectrometer, a lichen cover index was computed using the ratio from DAIS channels 17 (0.77 μm) /12 (0.68 μm). Using field spectra, an index to differentiate rock from soil was built using DAIS channel 27 (0.9470 μm), consistent with the outcrop areas most outstanding on thermal infrared, particularly sensitive to rock outcrops.

4.1. Field spectra

Field spectra using a GER Spectrometer on different granite facies and types do display simmilar absorption features for all granitic rocks (Fig. 2). The overall reflectance is maximum for white granite without biotite and coarse texture (heterogranular granite with muscovite). Soil, contrary to the imagery, display lower overall reflectance than light rocks (Fig. 2). The reason is that rock boulders used for field measurements are clean pieces of rock, which would never cover a reasonably wide area on the surface to be recorded by the imagery. Therefore, reflectances shown by the imagery from exposed weathered surfaces should be considered as more representative. Coarse grained rocks also show deep 2.2 μm absorptions due to the presence of muscovite, as well as soil (Fig. 2).

4.2. DAIS imagery

Iron oxides produced by weathering of biotite are spectrally present on DAIS Z profiles on rock outcrops and the skeletal dark regolith with the same intensity (Fig. 3), and with less expression on the inmediately more weathered regolith (thin light regolith). All the spectra showing iron contents in the visible also display a wide depression between 2 μm and 2.11 μm with a steep ascent up to 2.135 μm, and emphasized depression on 2.18 μm. Such features are absent on the loose material more claysh and quartziferous (thin claysh regolith, thick regolith, anthropogenic soil). The exception to the rule is the granite rock with pitting, showing a smooth ascent from 2.3 to 2.10 μm. Pitting seems to be responsible for such spectral difference.

From the four initial regolith areas spectrally distinct, granite soil with dry grass is most distinguishable from the rest with a steep decrease in reflectance from the nearinfrared to the middle infrared (Fig. 3). Influence of green or dry vegetation growing along the wetter lower areas where granite soil with dry grass is located is not shown in the visible, but a steep decrease in reflectance from the shortwave nearinfrared to the middle infrared is due to the presence of vegetation. The spectrally different areas found inside granite soil with dry grass on the imagery correspond to density or greenage of vegetation. The overall reflectance of this soil is the maximum for the whole scene on 0.98 μm, apart from the anthropogenic soil.

Lack of available energy on the fourth sensor in the middle infrared disguises any spectral features related to the presence of clay or carbonate. Nevertheless, spectra on regolith display minor nuances non existent on rock outcrop between 2 and 2.2 μm.

Areas of human influence as cultivated fields, or soil along roads display the highest overall reflectance on DAIS data.

4.3. Laboratory spectra on soil

Soil samples collected in the field on sites following patterns suggested by the imagery, are dry-sieved and submitted to measurement of diffuse reflectance in the laboratory with a

spectrometer provided with an integrating sphere. They show a very simmilar spectral response according to the distance to the outcrop to DAIS imagery. To ensure accuracy on soil colour appreciation, soil colour indexes (Munsell,1950) have been observed in the laboratory under a uniform illumination source. In every single granite facies considered, soil close to the outcrop (skeletal dark regolith) are darker in colour and lower in overall reflectance than the more evolved weathering and transported mixtures (thin light regolith, thick regolith) (Fig. 4).

The mineralogy of the four granite facies examined is also responsible for subtle spectral nuances. Abondance of feldspar on the rock results on more intense weathering. The granite facies with large feldspar phenoclasts offers the minimum exposed rock outcrop. Grus and lehnt cover nearly the whole surface covering the underlying rock. An obvious convex shape in the visible distinguishes this granitic facies, emphasized on thin claysh regolith and thick regolith (Fig. 4). It also displays a lighter colour (2.5Y 5/6, light olive brown), and high overall reflectance spectrally outstanding on the imagery.

The northern homogeneous granite with abondant feldspar and big muscovite and biotite crystals displays the larger area of outcrop, with less depressions with thick soil, and consequently, the least weathered granite facies. This is the reason why the soil is darker (2.5Y 4/4, olive brown, 2.5Y 5/2 grayish brown). The presence of biotite results on a slight concave shape on the visible due to the presence of iron oxides produced by the weathering of biotite, emphasized on the spectra from thick regolith, gathering the mineralogical products in advanced stages of weathering.

The deformed granite with feldspar and biotite presents the largest area of outcrop. Intense weathering concentrates along fractures. Loose material shows an average light olive brown colour (2.5Y 5/3), the darkest colour and lower overall reflectance from all the granite facies considering every mineralogical association and soil thickness. It joins spectrally the homogeneous northern granite with biotite and muscovite on the slightly concave shape in the visible due to the presence of iron oxides (Fig. 4).

The coarse grained homogeneous granite with large quartz crystals displays a high overall reflectance and lack of spectral features associated both to abondance of biotite and feldspar (2,5Y 4/3, 4/4, olive brown; 2.5Y 5/3, light olive brown).

According to Escadafal (1989), the medium Munsell value recorded for soil colour is related to overall reflectance. This is true for the four granite facies considered and particularly true for the sequence of mineralogical associations away from the outcrop line from skeletal dark regolith to thick regolith.

No difference has been recorded at 2.2 μm related to abondances of biotite and muscovite (Riaza et al, 1993). Deep weathering of both filosilicates hinders their spectral expression in the nearinfrared.

To summarize, high overall reflectance corresponds to thick claysh regolith on every granite facies. The presence of clay and thick texture prevents water from infiltrating the soil in depth. Iron minerals favour the development of crusts acting as a barrier to water infiltration. However, spectral properties restrict the presence of iron bearing minerals to rock outcrops and the loose material in their inmediate neighbourhood, located on geomorphologically elevated areas, where water drains superficially. Therefore, only soil clay contents seems spectrally critical in relation to soil water infiltration.

5. Spectral behaviour of rocks and soils in thermal infrared, day and night

The spectral behaviour of mapped areas in the thermal infrared is suggestingly different between day and night data (Fig. 6). Apart from water, the most extreme high emmissivity on night thermal infrared data, rock outcrops are clearly distinguished spectrally from various grus mixtures on the soil on night emmissivities. Again, pitting with outstanding quartz grains and likely the presence of lichen on holes and surfaces of the rock, are responsible for the spectral response of rock outcrops on the night thermal infrared data.

Both rock and soil behave with opposite spectral responses on day and night data (Figs. 5 and 6). Digital image processing using both day and night data enhances nuances on their spectral behaviour. Minimum noise fraction transforms and principal component analysis on data which have been masked isolating wether rock or soil on areas devoid of vegetation are the most efficient treatments differentiating data.

Wide areas of rock outcrop are clearly distinguished from the rest on the colour composites. Pitting seems to be responsible for outstanding responses on thermal infrared both day and night (Figs. 5 and 6), due to the irregular texture of the surface producing cavity radiation effects (Kahle et al, 1988). This way, the coarse grained homogeneous granite with a wide area of outcrop is more clearly shown on thermal infrared images.

When considering the spectral response of individual granite facies based on selected spectrally homogeneous areas on the imagery, it is the granite with feldspar phenoclasts the most different (Fig. 5) both on day and night data. Abondance of clay minerals on the very homogeneously weathered surface produces high responses on thermal infrared day data, corresponding to a fairly light soil (2.5Y 5/6, light olive brown).

The rock outcrops of deformed granite with feldspar are particularly outstanding on night data. Again, cavity effects due to heterogeneous surfaces due to deeper weathering of feldspar grains are responsible for high night emittance on the thermal infrared.

6. Conclusions

Hyperspectral imagery helps to map the weathering front on granite, and different degrees of weathering on rock. Field spectra have been used to compute a lichen cover index on rock, and different masks isolating soil and vegetation, in order to increase separability among every geological and land cover unit. Different mineralogical associations and soil grain size and packing on grus and lehnt produced by weathering are spectrally recorded related to intensity of weathering processes on regolith. Such differences are varyingly displayed depending on the

original mineralogy, texture and fracturing pattern of the rock, summarized by its geomorphology.

Granite rock more intensely deformed is prone to faster weathering than homogeneous nonstressed textures. Areas with more regolith and more intense weathering mineral associations correspond to intensely deformed granite outcrops. However, fracturing favours intense weathering in depth leaving wider area of relatively fresh outcrop on the surface.On homogeneous textures, the presence of biotite is critical for the spectral expression of mineralogical weathering products as iron oxides, and their associated clays, resulting on a decreasing convexity of the spectral measurements in the visible. Abundance of clays results on low soil water infiltration capability, considered as the most spectrally critical parameter on the area, indicating areas where pools of standing water form after the rainy season.

Pitting on fresher rock outcrops as quartz grains remaining in relief is responsible for the outstanding spectral response in the visible and nearinfrared, masking spectral contributions from feldspar and mica which have been dissolved. Texture rather than mineralogy contributes to the spectral response of the rock surface.

Rocks and soils behave with opposite emittance ranges on thermal infrared day and night data. Rock outcrops with rugged surfaces due to abondance of quartz grains or relative abondance of weathered feldspar show emphasized responses on thermal infrared, both day and night data, due to the cavity radiation effect.

Rock outcrops are spectrally distinguished from various grus mixtures on the soil, whose colour lightens and overall reflectance increases with the distance to the rock outcrops in the visible and nearinfrared. Rock and soil maps produced by image processing of hyperspectral data following the above considerations can suggest soil particle size distribution, soil aggregation, soil depth, and consequently, be useful on the elaboration of soil loss and soil conservation maps.

7. Acknowledgement

This work has been funded by the Training and Mobility Program from the Department of Education and Science in Spain. The DAIS Large Scale Facility based at the German Aerospace Research Establishment (DLR), in the environmental section of the program "Training and Mobility of Researchers" from the European Community Directorate General XII has been the host of the joint activity. L. Pascual, from the Institute of China and Glass (CSIC, Madrid) has helped with the use of the laboratory spectrometer. Estudio Atlas provided a licence of the image processing software ENVI.

8. References

Abrams, M. Abbott, E. and Kahle, A., 1991. Combined Use of Visible, Reflected Infrared, and Thermal Infrared Images for Mapping Hawaiian Lava Flows, Journal of Geophysical Research, 96, NO. B1: 475-484.

Clark, R. N., Swayze, G. A., Gallagher, A., King, T. V. V. and Calvin, W. M., 1993. The U.S. Geological Survey Digital Spectral Library: Version 1: 0.2 to 3.0 mm: U.S. Geological Survey, Open File Report 93-592.

Escadafal, R., Girard, M-C. y Courault, D., 1989. Munsell Soil Color and Soil Reflectance in the Visible Spectral Bands of Landsat MSS and TM Data, Remote Sensing of Environment, 27: 37-46.

Evans, R., 1980. Mechanics of water erosion and their spatial and temporal controls: an empirical viewpoint, in, Ed. Kirkby , M.J., and Morgan, R.P.C., Soil Erosion, Chichester (UK), John Wiley and Sons, pp.109-128.

Grove, C. I., Hook, S. J., and Paylor II, E. D., 1992. Laboratory Reflectance Spectra of 160 Minerals, 0.4 to 2.5 Micrometers: Jet Propulsion Laboratory Publications, pp. 92-2.

Hill, J., 1993. Land degradation and soil erosion hazard mapping in mediterranean environment with operational earth observation satellites, Proceedings International Symposium "Operationalization of Remote Sensing", 19-23 April 1993, Enschede, The Netherlands, vol.9: 41-52.

Johnson, J.R., Lucey, P.G., Horton, K.A., Winter, E. M., 1998ª. Infrared Measurements of Pristine and Disturbed Soils 1. Spectral Contrast Differences between Field and Laboratory Data, Remote Sensing of the Environment, 64: 34-46.

Johnson, J.R., Lucey, P.G., Horton, K.A., Winter, E. M., 1998b. Infrared Measurements of Pristine and Disturbed Soils 2. Environmental Effects and Field Data Reduction, Remote Sensing of the Environment, 64: 47-52.

Kahle, A.B., Gillespie, A.R., Abbott, E.A., Abrams, M. J., Walker, R. E., and Hoover, G.,1988. Relative Dating of Hawaiian Lava Flows Using Multispectral Themal Infrared Images: A New Tool for Geologic Mapping of Young Volcanic Terranes, Journal of Geophysical Research, 93, B12: 15239-15251.

Müller, A. and Oertel, D., 1997. DAIS Large-Scale Facility, the DAIS 7915 Imaging Spectrometer in an European Frame, Proceedings of the Third International Airborne Remote Sensing Conference and Exhibition, 7-10 July 1997, Copenhagen, Denmark, vol.I: 684-691.

Munsell Color Co. (1950, reviewed 1975), Munsell Soil Color Charts, Munsell Color, Macbecth Division of Kollmorgen Corporation, Baltimore, (MD, United States).

Ninomiya, Y., Matsunaga, T., Yamaguchi, Y., Ogawa, K., Rokugawa, S., Uchida, K., Muraoka, H. and Kaku, M., 1997. A comparison of thermal infrared response spectra measured in situ, in the laboratory, and derived from thermal infrared multispectral scanner (TIMS) data in Cuprite, Nevada, U.S.A. International Journal of Remote Sensing, 18, n°7: 1571-1581.

O´Neill, A. L., 1994, Reflectance Spectra of microphytic soil crusts in semi-arid Australia, International Journal of Remote Sensing, vol.15 nº3: 675-681.

Riaza, A., 1992. Reflectancia en rocas en función de su litología y fábrica interna. II Cartografía de rocas ígneas en el Complejo de Burguillos del Cerro en el visible y el infrarrojo cercano: reflectancia espectral en el laboratorio y evaluación estadística de la misma en relación con imágenes thematic mapper, Boletín Geológico y Minero, 103, n°3: 3-26.

Riaza, A., Escuder, J., Villar, P., Martin Alfageme, S., 1993. Remote Sensing on Geological Mapping on an Igneous and Metamorphic Complex (Salamanca, Spain), Proceedings International

Symposium "Operationalization of Remote Sensing", 19-23 April 1993, Enschede, The Netherlands, vol.9: 113-124.

Riaza, A., Mediavilla, R., Santisteban, J. L., Villar, P. and Martín Alfageme, S., 1995. Regolitos en una cuenca terciaria. Propiedades espectrales según su mineralogía en función de la evolución climática, Coloquio Internacional sobre propiedades espectrales y teledetección de los suelos y rocas del visible al infrarrojo medio, La Serena (Chile), 24-27 de April 1995, pp. 100-104.

Riaza, A., Mediavilla, R., and Santisteban, J.I., 2000, Mapping geological stages of climate-dependent iron and clay weathering alteration and lithologically uniform sedimentary units using Thematic Mapper imagery, International Journal of Remote Sensing, vol.21, nº5: 937-950.

Richter, R., 1996. Atmospheric correction of DAIS hyperspectral image data, Computers & Geosciences, vol.22, no.7: 785-793.

Rollin, E.M., Milton, E.J., and Roche, P., 1990. The influence of lichen on the reflectance spectra of granitic rocks, Proceedings of the 16th Annual Conference of the Remote Sensing Society, University College of Swansea, 19th-21st September 1990, Swansea, United Kingdom, pp. 368-377.

Salisbury, J. W., Walter, L. S., Vergo, N. and D'Aria, D. M. 1992. Infrared (2.1-25 μm) Spectra of Minerals, The John Hopkins University Press, Baltimore (Maryland, USA).

Salisbury, J.W., 1992. Infrared (8-14 μm) Remote Sensing of Soil Particle Size, Remote Sensing of the Environment, 42: 157-165.

Stoner, E.R. and Baumgardner, M.F., 1981. Characteristic Variations in Reflectance of Surface Soils, Soil Science Society of America Journal, 45: 1161-1165.

Strobl, P., Richter, R., Lehman, F., Müller, A., Zhukov, B., Oertel, D., 1996. Preprocessing for the Digital Airborne Imaging Spectrometer DAIS 7915, SPIE´s AEROSENSE ´96 Conference, Orlando, Apr. 8-12, 1996, SPIE Proc. Vol. 2758.

Twidale, C.R., 1982. Granite landforms, Elsevier, Amsterdam.

Fig.1.- DAIS 7915 images used to elaborate a map: A: false colour composite with channels 20, 39 and 54 (blue, red, green) in the visible and nearinfrared. B: colour composite with principal components second, first and fourth (blue, red, green) computed on five selected channels in the visible and nearinfrared after masking water and vegetation influence, to enhance differences on rocks and soil. C: Rock and soil map elaborated after a maximum likelihood classification using training areas defined based on observations on various colour composites.

Fig.2 . Field spectra taken with a GER Spectrometer in the visible and near-infrared (0.4-2.4 μm) for various granitic facies and soil.

Fig.3. Z profiles for DAIS channels in the visible and near-infrared for outcrops and regolith from homogeneous areas shown spectrally on the imagery, and different vegetation cover.

Fig.4. Laboratory spectra in the visible and near-infrared (0.4-2.4 μm) from soil samples collected on areas indicated by the imagery for the different soil classes according to weathering mineralogy developed on four granite facies.

Fig.5. Rocks and soils behave in opposite emittance ranges on thermal infrared day and night data. Rock outcrops with more rugged surfaces due to abondance of quartz grains or relative abondance of weathered feldspar show emphasized responses on thermal infrared, both day and night data, due to the cavity radiation effect.

Fig.6. Thermal infrared registered day and night data are evaluated through principal components analysis and minimum noise fraction transforms to enhance separability criteria after masking for soil and rock. A: Colour composite on thermal infrared on rock areas using minimum noise fraction transforms 7 (red) 1 (green) and 3 (blue). B: Colour composite on thermal infrared on soil areas using minimum noise fraction transforms 1 (red) 2 (green) and principal component 2 (blue). C. Map on different granite facies for rock and soil developed after observations on the prior imagery.

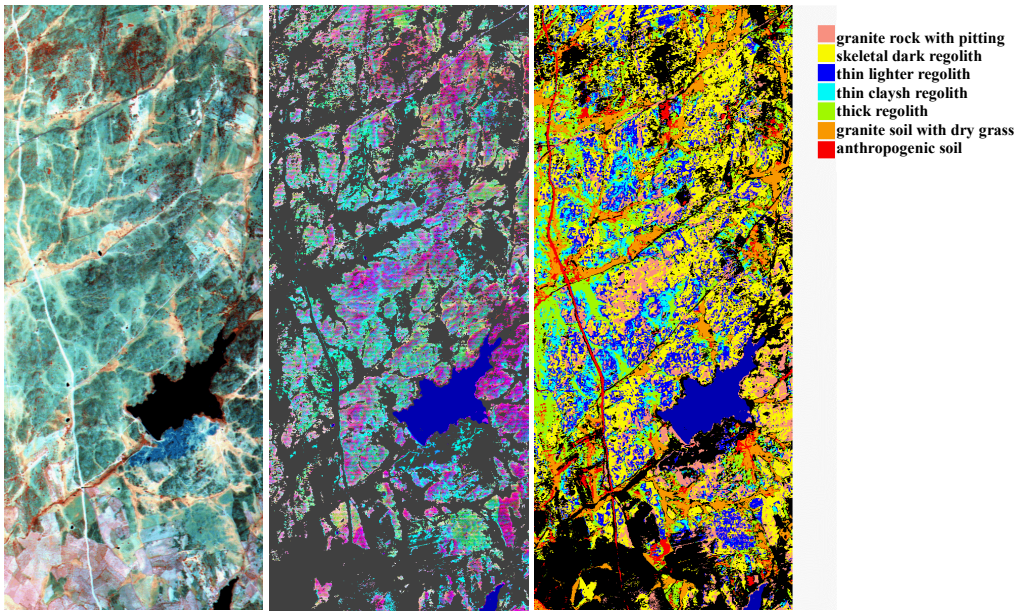

Fig.1.- DAIS 7915 images used to elaborate a map: A: false colour composite with channels 20, 39 and 54 (blue, red, green) in the visible and nearinfrared. B: colour composite with principal components second, first and fourth (blue, red, green) computed on five selected channels in the visible and nearinfrared after masking water and vegetation influence, to enhance differences on rocks and soil. C: Rock and soil map elaborated after a maximum likelihood classification using training areas defined based on observations on various colour composites.

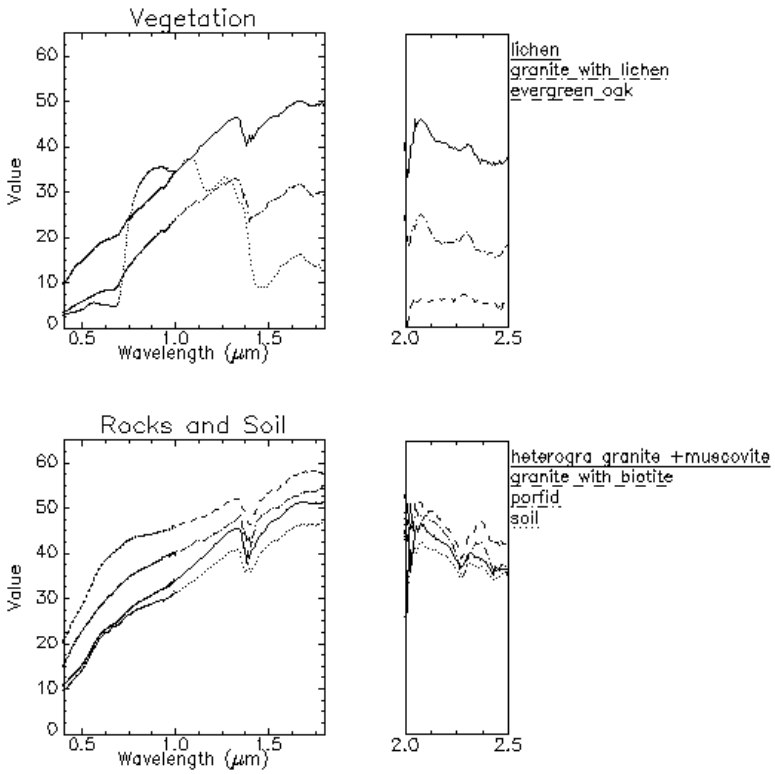

Fig.2 . Field spectra taken with a GER Spectrometer in the visible and near-infrared (0.4-2.4 μm) for various granitic facies and soil.

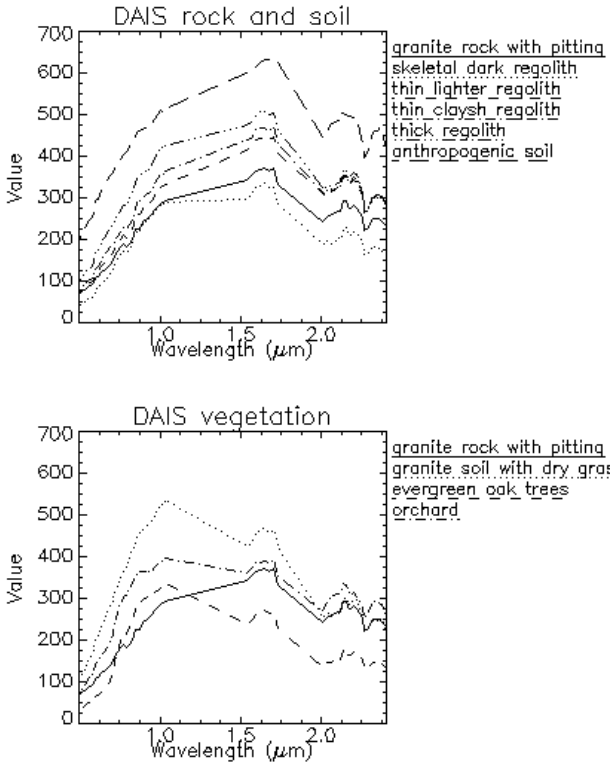

Fig.3. Z profiles for DAIS channels in the visible and near-infrared for outcrops and regolith from homogeneous areas shown spectrally on the imagery, and different vegetation cover.

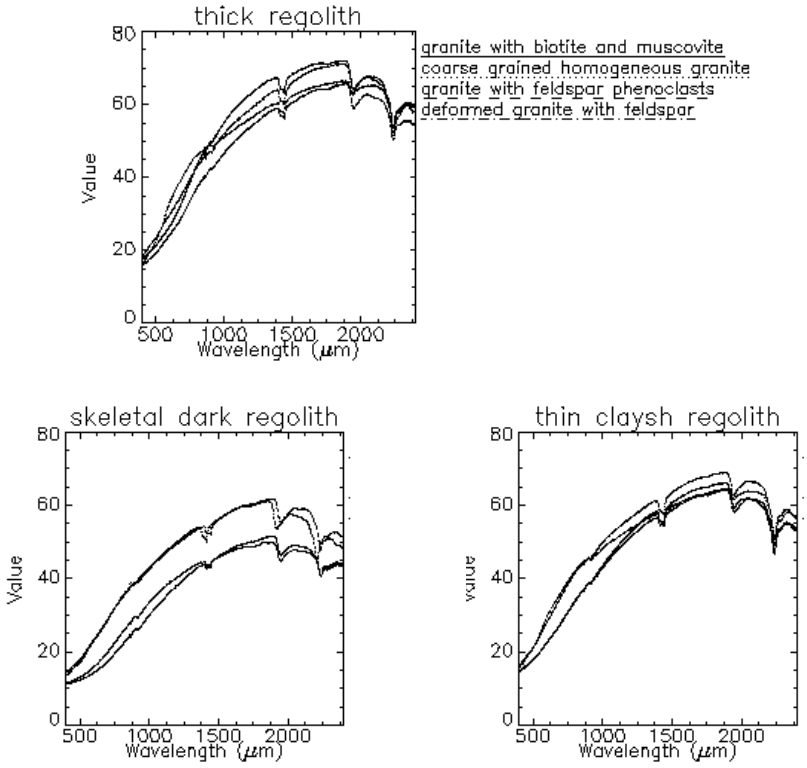

Fig.4. Laboratory spectra in the visible and near-infrared (0.4-2.4 μm) from soil samples collected on areas indicated by the imagery for the different soil classes according to weathering mineralogy developed on four granite facies.

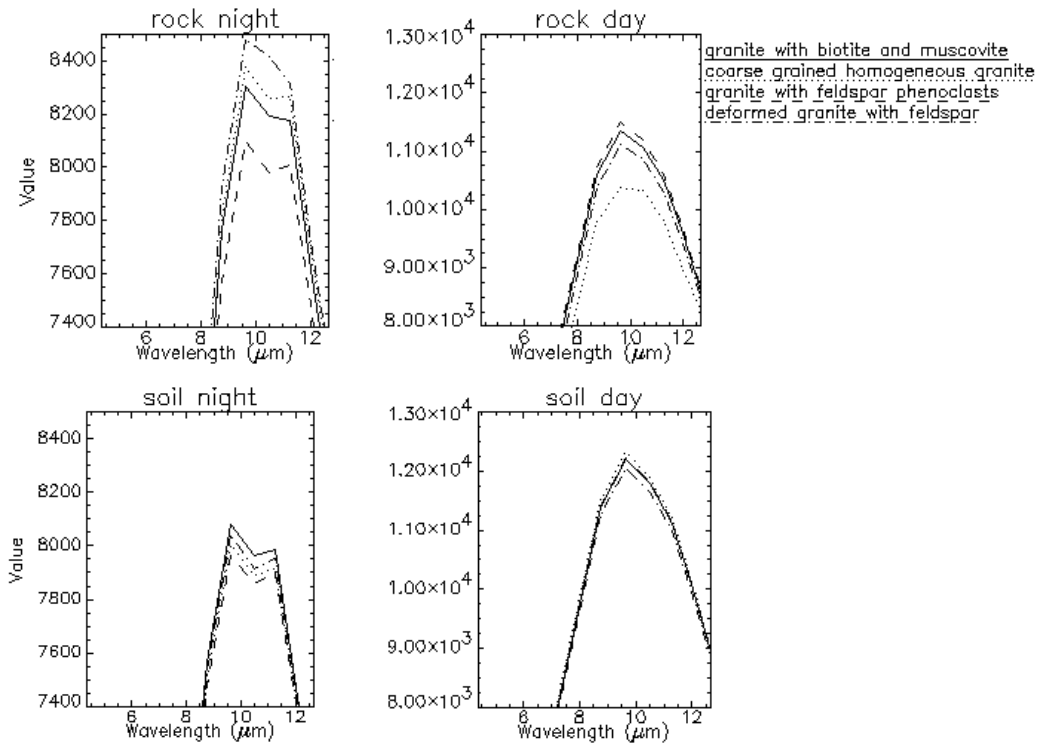

Fig.5. Rocks and soils behave in opposite emittance ranges on thermal infrared day and night data. Rock outcrops with more rugged surfaces due to abondance of quartz grains or relative abondance of weathered feldspar show emphasized responses on thermal infrared, both day and night data, due to the cavity radiation effect.

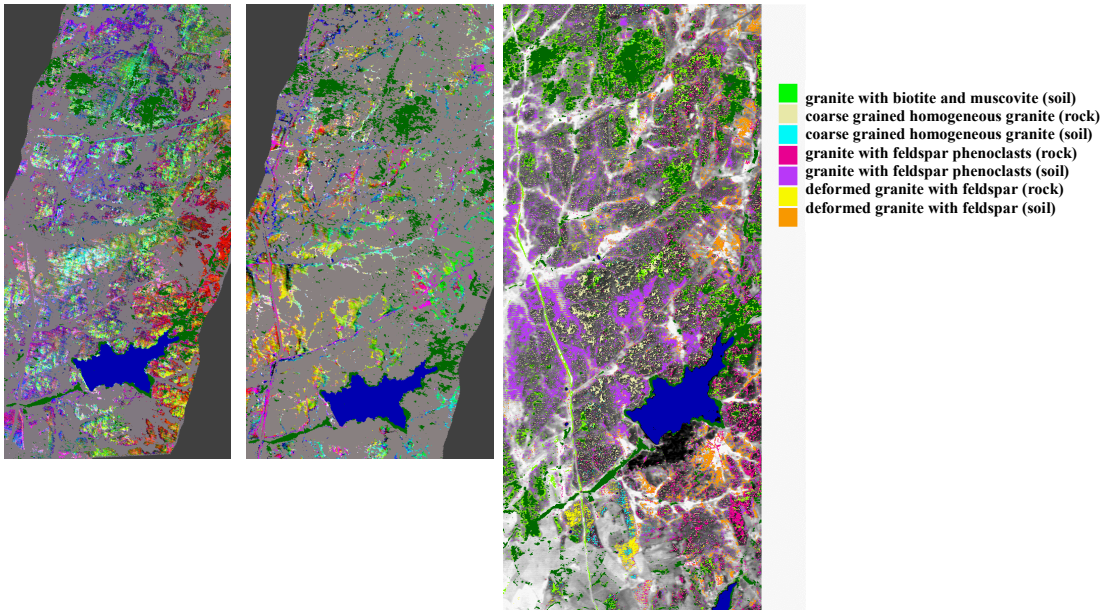

Fig.6. Thermal infrared registered day and night data are evaluated through principal components analysis and minimum noise fraction transforms to enhance separability criteria after masking for soil and rock. A: Colour composite on thermal infrared on rock areas using minimum noise fraction transforms 7 (red) 1 (green) and 3 (blue). B: Colour composite on thermal infrared on soil areas using minimum noise fraction transforms 1 (red) 2 (green) and principal component 2 (blue). C. Map on different granite facies for rock and soil developed after observations on the prior imagery.